Journal of Alloys and Compounds 842 (2020) 155983

Contents lists available at ScienceDirect

Journal of Alloys and Compounds

journal homepage: http://www.elsevier.com/locate/jalcom

# The electronic structure, transport and structural properties of nitrogen-decorated graphdiyne nanomaterials

İskender Muz [a], Mustafa Kurban [b, *]

[a] Department of Mathematics and Science Education, Nevşehir Hacı Bektaş Veli University, 50300, Nevşehir, Turkey
[b] Department of Electronics and Automation, Kırşehir Ahi Evran University, 40100, Kırşehir, Turkey

ARTICLE INFO

*Article history:*
Received 26 February 2020
Received in revised form
29 May 2020
Accepted 6 June 2020
Available online 8 June 2020

*Keywords:*
Graphdiyne
Nitrogen-doped
Nanomaterials
DFT
DFTB

ABSTRACT

We focus on a theoretical investigation using the DFT and LC−SCC−DFTB for investigating the structural, optical and reactivity properties and electronic structure of pristine graphdiyne (GDY) and nitrogen (N)-doped hexagonal carbon rings of GDY nanomaterials. Our calculations show that the energy gap ($E_g$) of the GDY is 1.00 eV which is excellent agreement with the DFTB. By increasing the content of N, the $E_g$changes in the wide range of 0.15−0.98 eV. The absorbance maxima are at 1.91 eV (647 nm) for the GDY, 1.46 eV (845 nm) for the N-GDY, 2.15 eV (576 nm) and 1.21 eV (1020 nm). The decrease in the value of the $E_g$with temperature for the GDY and 3 N GDY is observed due to variations of the bond energy which reflects the $E_g$. However, an increase in the value of the $E_g$with temperature is found linearly for the N-GDY because the Fermi energy level is pushed higher from −3.722 to −4.027 eV. The dipole moment increases when increasing the content of N and temperature. Obtained results herein suggest the GDY and N-doped GDY nanomaterials can be used as very promising advancements for potentially useful optoelectronic novel applications.



## 1. Introduction

Recently, carbon-based materials have found use in many areas such as energy, electronics, biomedical, optical fields, etc. Among them, Graphdiyne (GDY) has received extensive attention, due to its fascinating properties such as unique two-hybrid state (sp-sp$^2$), uniform pores, and highly π-conjugated structure [1,2]. These properties provide promising potential in diverse fields of applications such as lithium-ion storage [3], nanocomposite photocatalyst [4], the anode of lithium and rechargeable batteries [5,6], clean energy [7], spintronics [8,9], and so on.

GDY, which has been grown on the surface of copper (Cu) via a cross-coupling reaction [10], is a novel 2D non-natural carbon allotrope containing hexagonal carbon rings connected by diacetylene bonds [1]. GDY has a bandgap of 0.46 eV and exhibits high carrier mobility at room temperature [11]. GDY also has a high Seebeck coefficient and electrical conductivity as well as low thermal conductivity [12]. In addition to the applications mentioned above, a GDY-based electrochemical actuator with a high electromechanical transduction efficiency of up to 6.03% was fabricated [13]. GDY electrode has recently been searched for electrochemical supercapacitor [14]. The ultrathin GDY nanofilms significantly improve the coulombic efficiency and long-term cycling performance of Li metal battery [15]. Also, integrating ultrathin GDY nanomaterial on silicon electrodes exhibited high-performance silicon anode [16]. The photocatalytic properties of a novel GDY-ZnO nanohybrid were examined on the degradation of methylene blue and rhodamine B [17]. Nowadays, it is a hot topic to control and utilize the electronic properties and chemical activities of carbon-based nanomaterials with doping of a foreign atom [18].

The previous studies show that nitrogen (N)-doped CBNs have been preferred in general, because the electrons can be injected into the materials by N atom [19] and thus tuning the electrical transport properties. Up to now, N-doped CBNs have been extensively studied both theoretically and experimentally [20−24]. On the other hand, many studies show that N-doped GDY has more desirable properties than undoped GDY. For example, dopant N gives rise to an increase in the performance of GDY electrochemical electrodes for new energy fields, such as fuel cells, batteries, solar cells, Li/Na-ion capacitors [25,26] where the layered and porous N-doped GDYs are carried out. Also, selectively N-doped GDY and porous GDY can be used as excellent metal-free catalysts for oxygen

* Corresponding author.
*E-mail addresses:* mkurbanphys@gmail.com, mkurban@ahievran.edu.tr (M. Kurban).

https://doi.org/10.1016/j.jallcom.2020.155983
0925-8388/

reduction [27,28]. A recent study showed the local structures of N-doped GDY based on computational X-ray spectroscopy [29]. On the best of our knowledge, there is no similar work for N-doped at different sites the 6C-hexagon of GDY. Hence, we have performed N-doped at different sites of GDY nanomaterials to figure out its structural, electronic, optical and reactivity properties and to compare to the undoped GDY. It is important to note that three different doping positions of N atom on the pristine GDY were studied because the GDY undergoes a large deformation after the addition of more than three nitrogen atoms to 6C-hexagon. We calculated the binding energy, formation energy, ionization energy, electron affinity, HOMO, LUMO, HOMO-LUMO energy gap, density of state, charge distribution, electron localization function, the quantum chemical descriptors such as chemical hardness and potential, maximum amount of electronic charge index, and electrophilicity index by density functional theory (DFT). We also analyzed the UV–visible absorption spectra and optical energy gap using time-dependent (TD)-DFT. The obtained results also compared with the long-range corrected self-consistent charge density-functional based tight-binding (LC–SCC–DFTB) method. Molecular dynamics simulations (MD) have also been performed to research temperature-dependent physical properties of the GDY and N-doped GDY nanomaterials. Our results show that N-doped GDY is a potential candidate for optoelectronic applications.

## 2. Computational details

The structural relaxation of pristine graphdiyne (GDY) and nitrogen-doped graphdiyne (N-doped GDY) nanomaterials were carried out using the Gaussian 09 program [30] based on density functional calculation (DFT) [30]. During the relaxation process, reliable B3LYP [31,32] exchange-correlation functional with suitable split-valence basis set 6-31G(d) [33] was preferred. The GDY contains 72 carbons (C) and 12 hydrogens (H) atoms ($C_{72}H_{12}$), which was taken such as the basic building block of GDY, in the proposed model. Dangling bonds were capped with H atoms, and then GDY, N-GDY ($NC_{71}H_{12}$), 2N-GDY ($N_2C_{70}H_{12}$) and 3N-GDY ($N_3C_{69}H_{12}$) were fully relaxed.

The binding and formation energies are represented $E_b$and $E_f$, respectively and calculated as follows:

$$E_b = (n_C \times E_C + n_N \times E_N + n_H \times E_H - E_{total})/(n_C + n_N + n_H) \quad (1)$$

$$E_f = E_{N-doped\ \ GDY} + (n_{C-reduced} \times E_C) - \left(n_{N-doped} \times E_N\right) - E_{GDY} \quad (2)$$

where $E_{total}$, $E_{GDY}$ and $E_{N-doped\ \ GDY}$are the total energies of GDY or N-doped GDY. $E_C$, $E_N$ and $E_H$ are the total energies of C, N, and H atoms. $n_C$, $n_N$ and $n_H$ are the numbers of C, N and H atoms. The $n_{C-reduced}$ and $n_{N-doped}$ are the numbers of reduced C atoms and doped N atoms, respectively.

The vertical ionization potential (*VIP*) and vertical electron affinity (*VEA*) are calculated as follows: $[VIP = E^+ - E^0]$ and $[VEA = E^0 - E^-]$. Where *VIP* is defined as the difference between two energy levels the ground state of the cation ($E^+$) and the ground state of the neutral ($E^0$) at the geometry of the neutral. *VEA* is the difference between two energy levels the ground state of the neutral ($E^0$) and the ground state of the anion ($E^-$) at the geometry of the neutral.

The HOMO and LUMO energies can be given with respect to Koopman's theorem by $I \approx -E_{HOMO}$ and $A \approx -E_{LUMO}$. Thus, the quantum chemical descriptors including chemical hardness ($\eta$), chemical potential ($\mu$), electrophilicity index ($\omega$), maximum amount of electronic charge index ($\Delta N_{tot}$)can be calculated as follows [34,35]: $[\eta = (I - A)/2]$, $[\mu = -(I + A)/2]$, $[\omega = \mu^2/2\eta]$ and $[\Delta N_{tot} = -\mu/\eta]$ where $I$ and $A$ correspond to vertical ionization potential and vertical electron affinity, respectively.

GaussSum 2.2 program [36] is implemented to determine the density of states (DOS) and partial density of state (PDOS) plots. Also, TD-DFT calculation based on the CAM-B3LYP functional [37] and 6-31G(d) basis set has performed to predict UV–visible (UV–vis) absorption spectra and optical energy gap. The obtained results also compared with the LC–SCC–DFTB method implemented in DFTB + code [38]. MD simulations have been performed using DFTB with ob2-1-1/shift [39] set of Slater Koster parameters. The simulations use the Andersen thermostat [40] sampling an NVT ensemble. Verlet algorithm [41] was used for numerical integration with a time step length of 1 fs.

## 3. Results and discussions

### 3.1. Structural analysis

The geometries of the GDY, N-GDY, 2N-GDY, and 3N-GDY, which are completely optimized at the B3LYP/6-31G(d) level, are given in see Fig. 1 and Fig. S1 (in Supporting information). Besides, the point group symmetries (Symm.), electronic states (E.S.) and total energies ($E_{tot}$) of the GDY and N-doped GDY nanomaterials are also tabulated in Table S1 in Supporting information. The point group symmetry of GDY is a quasi-planar geometry with $C_{3V}$ (see Fig. 1) and it has $^1A_1$ (singlet) electronic state. The atomic framework of GDY can see to be C hexagons interconnected by acetylene $C \equiv C \equiv C = C \equiv C \equiv C$ chains. Due to hybridization in these chains, the CC near-neighbor bond distances along the chain are the following: 1.39, 1.22, 1.33, 1.22, and 1.40 Å, aligned from one C atoms of a hexagon to the nearest C of an adjacent hexagon. However, the CC near-neighbor bond distances in the hexagons are larger, with an average distance of 1.42 Å. These results are obtained with a very good precision comparing with the literature [42]. In addition, the structure of GDY contains 6C-hexagon and 18C-hexagon. For the GDY, the parallelogram with a broken line is plotted as a unit cell as

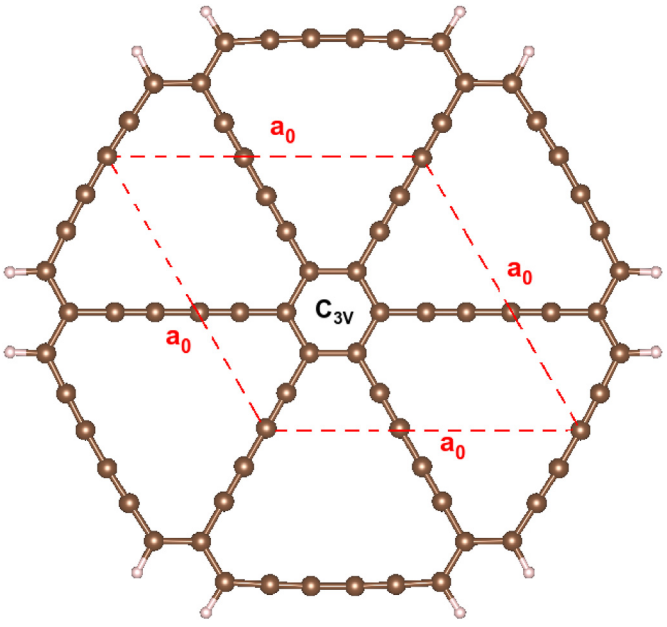


**Fig. 1.** (Colour online) The optimized structure of GDY at B3LYP/6-31G(d) level of theory. (For interpretation of the references to color in this figure legend, the reader is referred to the Web version of this article.)

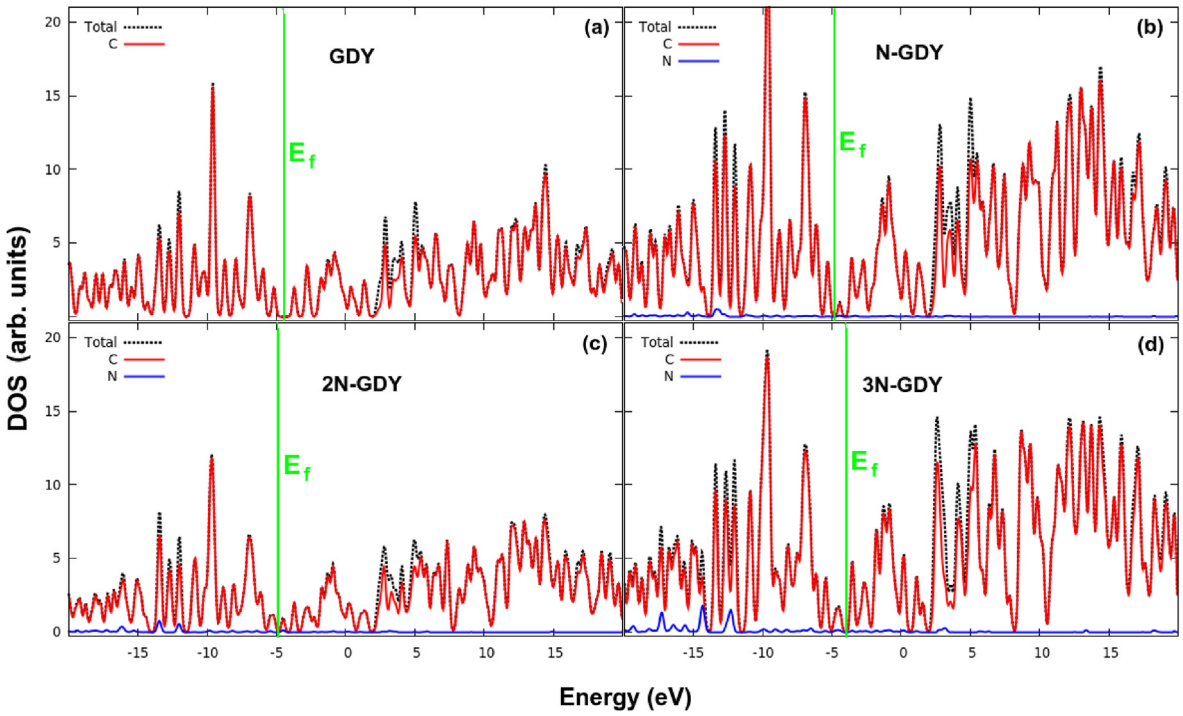


**Fig. 2.** (Colour online) The density of states (DOS) for the GDY and N-doped GDY nanomaterials. The black line, red line and blue line represent the density of the system, C atoms and N atoms, respectively. Green lines show the locations of the Fermi level. (For interpretation of the references to color in this figure legend, the reader is referred to the Web version of this article.)

seen in Fig. 1. The lattice constant or cell parameter for GDY is found to be $a_0 = 9.52$ Å (see in Fig. 1), in agreement with the previous values of 9.44–9.48 Å [11,43–47]. The point group symmetry of N-GDY is a planar geometry with $C_{2V}$ and it has $^2B_1$ (doublet) electronic state. Because a C atom is replaced by an N atom, structurally three different CCCCCC chains (seen in Fig. S1a as cyan, green, and orange colors) are formed for CC bond distances. Besides, the CC bond distances on the *CCCCCC* chains indicated by the same colors are equal and their bond numbers (single, double, and triple) are compatible with each other. In addition, hybridization continues as in GDY. The bond distances for the $N \cdots C{\equiv}C = C{\equiv}C \cdots C$ chain, where N atom is doped, are following: 1.34, 1.21, 1.35, 1.22, and 1.41 Å, aligned from one C hexagon to the nearest C of an adjacent hexagon. 2N-GDY has a planar geometry with $C_{2V}$ point group symmetry and $^1A_1$ (singlet) electronic state. Here, structurally two different *CCCCCC* chains (seen in Fig. S1b as cyan and green colors) are formed for CC bond distances due to the displacement of C atoms and N atoms. The CC bond distances on the *CCCCCC* chains indicated by the same colors are equal. The bond distances for the $N \cdots C{\equiv}C = C{\equiv}C \cdots C$ chains, where N atoms are doped, are the following: 1.33, 1.21, 1.35, 1.22, and 1.41 Å, aligned from one C hexagon to the nearest C of an adjacent hexagon.

3N-GDY belongs to the $C_{2V}$ point group with a planar geometry and $^2A_2$ (doublet) electronic state. Structurally two different *CCCCCC* chains (seen in Fig. S1c as cyan and green colors) are formed for *CC* bond distances due to the substitution of C atoms by N atoms. The *CC* bond distances on the *CCCCCC* chains indicated by the same colors are equal. The bond distances for the $N \cdots C{\equiv}C = C{\equiv}C \cdots C$ chains, where are doped N atoms, are the following: 1.34, 1.21, 1.35, 1.22, and 1.41 Å, aligned from one C hexagon to the nearest C of an adjacent hexagon.

The calculated binding energy per atom ($E_b$) for the GDY and N-doped GDY nanomaterials is tabulated in Table S1. The $E_b$ value of GDY is calculated to be 7.64 eV, in good agreement with previous studies [43,48]. Moreover, $E_b$ decreases slightly from 7.64 eV to 7.53 eV when N atoms are doped to pristine GDN (see Table S1). The $E_b$ of the GDY and N-doped GDY nanomaterials is found to be in the following decreasing order: GDY > N-GDY > 2N-GDY > 3N-GDY. This indicates that the pristine GDY is slightly more stable than N-doped GDY. In addition, the formation energies ($E_f$) of N-doped GDY are lie in the range of −2.85 and −3.42 eV, are very close to each other (see Table S1).

### 3.2. Electronic and reactivity properties

The density of state, charge distribution, ionization potential, electron affinity, HOMO and LUMO energies are some of the most fundamental electronic properties of nanomaterials. Fig. 2(a–d) shows the density of states (DOS) of GDY and N-GDY, which is calculated in the energy range −20 to 20 eV. The peak maximum in different energy intervals is noticed due to the overlapping of C atoms in the acetylene linkages along the GDY. The nitrogen (N) substitutions on GDY enhance the DOS at the Fermi energy level and cause the decrease of energy gap, thus increase the conductivity of GDY. Also, they are promising conditions for the possible use of chemical nanosensors. In addition, a change in the peak maximum for N-GDY occurs due to the transfer of charge between C and N atoms.

Fig. S3 and Fig. 3(a–f) show the partial density of states (PDOS) of s and p levels of C and N atoms for the GDY and N-GDY in the energy range −20 to 20 eV, respectively. The contribution of C atoms for GDY is presented in Fig. S3 where it can be obviously seen that only $p_y$ and $p_z$ orbitals for C atoms contribute to both valence band (VB) and conductance band (CB), whereas $p_x$ orbitals have no contribution. Also, the contribution from $p_x$ orbitals is more than $p_y$ and $p_z$. These results are also supported by the previous results [45,46]. The contributions of C for N-doped GDY are presented in Fig. 3(a, c, e). All the *p*-orbitals of C are contributing to both the VB

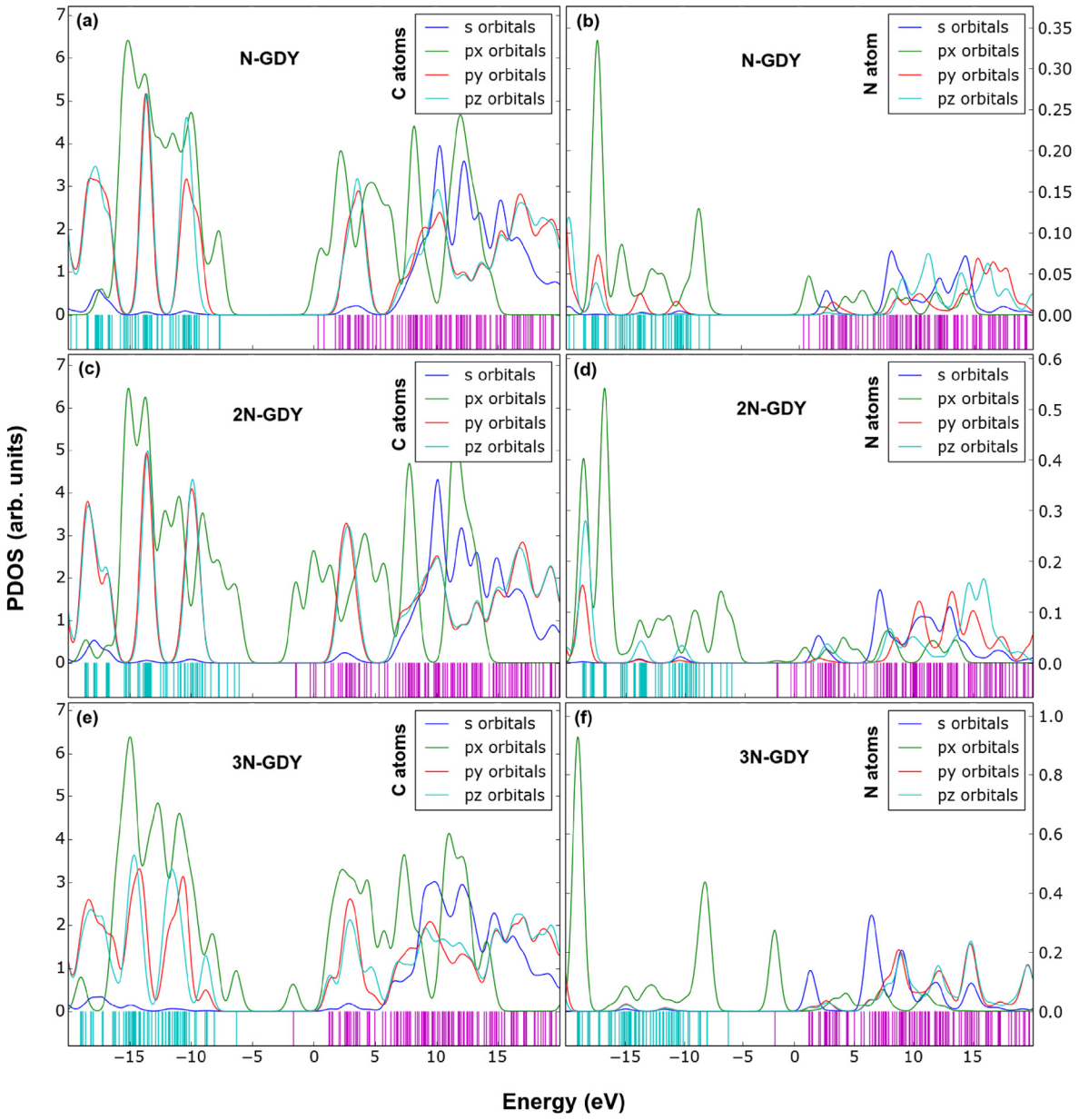


**Fig. 3.** (Colour online) The partial density of states on the s (blue), $p_x$ (green), $p_y$ (red) and $p_z$ (cyan) levels of C and N atoms for N-doped GDY nanomaterials is represented. (For interpretation of the references to color in this figure legend, the reader is referred to the Web version of this article.)

and CB, and the contribution from $p_x$ orbitals is more than $p_y$ and $p_z$. The contributions of C atoms for the GDY and N-doped GDY nanomaterials are presented in Fig. S3 and Fig. 3(a, c, f). Figs. show that all the *p*-orbitals on C contribute to both the VB and CB. In the case of N atoms, mostly $p_x$orbitals contribute to basically VB, and the contribution of $p_x$increases with increasing the content of N atoms (see Fig. 3(f)). However, the contribution from $p_y$ and $p_z$ orbitals for the VB is too small. In addition, *p*-orbitals of N atoms contribute less to the CB than that of the VB.

The natural population analysis of the GDY and N-doped GDY nanomaterials are shown in Figs. S2(a–b) in Supporting Information. We compared the effects of charge in the case of displaced C atoms with N atoms. Figs. S2(a–b) show that the N atoms carry a high negative charge (red rectangles indicated). However, each C atom bound three nearest C atoms has a small number of positive charges (green rectangles indicated). This is considered to be mainly because of the negatively charged on the basis of N atoms which causes the electrostatic charge distribution. The charges of C atoms in the range of −0.238 and −0.251 |e| at the corners (green circles indicated), where H atoms are captured by C atoms, are higher than that of other C atoms (see Figs. S1a–S1b). Here, the charge transitions are from H atoms to C atoms.

The HOMO-LUMO energy gap ($E_g$) for the GDY and N-doped GDY nanomaterials is tabulated in Table 1. The$E_g$of GDY is predicted as 1.00 eV and 1.03 eV using DFT and LC–SCC–DFTB calculations, respectively, which are in excellent agreement with the literature [42,49–52]. It can be comparable to the$E_g$of Si (1.14 eV), GaAs (1.43) and CdTe (1.5 eV) materials and recommends potential applications of GDY to be the supersede of these materials as a new semiconductor [53]. According to experimental results, the conductivity of GDY is reported in the range of $2.5 \times 10^{-4}$ and $3.2 \times 10^{-4}$ S/m, which is also similar to that of silicon [54,55]. It

**Table 1**
Electronic and reactivity properties of GDY and N-doped GDYs. All values are in eV. (All values are from DFT calculations except for $E_g$* which is obtained from LC–SCC–DFTB calculations).

| | GDY | N-GDY | 2N-GDY | 3N-GDY |
|---|---|---|---|---|
| VIP | 5.92 | 5.21 | 5.31 | 5.54 |
| VEA | 2.95 | 2.78 | 2.97 | 2.86 |
| HOMO | −5.20 | −4.35 | −4.43 | −4.86 |
| LUMO | −4.20 | −4.20 | −4.21 | −3.88 |
| $E_g$ | 1.00 | 0.15 | 0.22 | 0.98 |
| $E_g$* | 1.03 | 0.12 | 0.21 | 0.25 |
| $\eta$ | 1.49 | 1.22 | 1.17 | 1.34 |
| $\mu$ | −8.88 | −7.98 | −8.28 | −8.39 |
| $\omega$ | 26.52 | 26.23 | 29.30 | 26.26 |
| $\Delta N_{tot}$ | 5.98 | 6.57 | 7.08 | 6.26 |

also indicates that the porous GDY has a low carrier barrier which can be properly prepared under the experimental conditions. On the other hand, previous studies have pointed out that with N-doping, the electronic character of carbon nanotubes changes from semiconductor to conductor [56–58]. Therefore, it is very important how the N doping affects the$E_g$of the GDY. The $E_g$ decreases significantly from 1.00 eV to 0.15 eV when an N atom is doped to pristine GDN. However, when two (for 2N-GDY) and three (for 3N-GDY) N atoms are doped, $E_g$ increases to 0.22 eV and 0.98 eV, respectively (see Table 1). The similar trend was observed with LC–SCC–DFTB method. For example, the$E_g$for N-GDY is 0.12 eV, i.e., about 0.03 eV smaller than DFT calculations. Similarly, it is predicted for 2N-GDY as 0.21 eV, i.e., about 0.01 eV smaller than DFT. The increasing trend for 3N-GDY is also observed both the DFT and LC–SCC–DFTB methods. From the results, it is significant to note that N-GDY could be used as an electron transport material.

Global reactivity descriptors such as $\eta$, $\mu$, $\omega$and$\Delta N_{tot}$ defined in methodology part which are some of the most fundamental reactivity properties of nanomaterials, are given in Table 1. The VIP of the GDY is predicted to be 5.92 eV (see Table 1). Moreover, VIP decreases with N doping, but it increases from 5.21 to 5.54 eV when the number of doped N atoms increases. Thus, VIP is found as in the following decreasing order: GDY > 3N-GDY > 2N-GDY > N-GDY. The VEA value of GDY is found to be 2.95 eV (see Table 1). In addition, VEA exhibits oscillation behavior, but does not significantly affected by N doping. The $\eta$ value of the GDY is calculated to be 1.49 eV. With doping N, the $\eta$ values of the GDY and N-doped GDY nanomaterials vary between 1.22 and 1.34 (see Table 1). Similarly, $\omega$ and $\Delta N_{tot}$ values vary slightly with N-doping, whereas 2N-GDY is slightly higher than N-GDN and 3N-GDN. It also points out that 2N-GDY has a high tendency to accept electron(s). This is considered to be mainly because it has a closed-shell electronic configuration. Comparing to electronic and reactivity properties, pristine GDY is slightly more stable than N-doped GDN.

### 3.3. Optical properties

Absorption spectra and optical energy gap ($E_g^{opt}$)are some of the most fundamental optical properties of nanomaterials. Ultraviolet–visible (UV–vis) absorption spectra for the GDY and N-doped GDY nanomaterials are calculated by using time-dependent DFT (TD-DFT) and given in Fig. 4. The maximum UV–vis absorption spectrum value of GDY indicates an absorption peak located at 647.8 nm (around 1.9 eV) in the visible light region, which is good agreement with experimental results [2,59,60]. Moreover, it is shown that 2N-GDY is observed at a wavelength of 576.3 in the visible light region, whereas N-GDY and 3N-GDY give an absorption

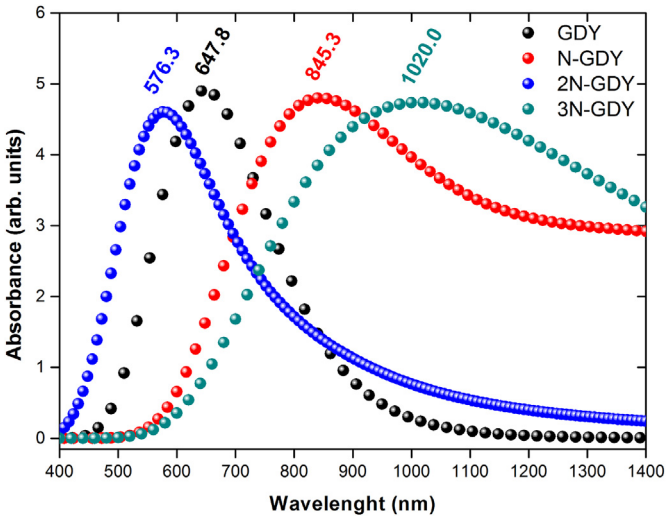


**Fig. 4.** (Colour online) The UV–visible absorption spectra of the GDY and N-doped GDY nanomaterials. (For interpretation of the references to color in this figure legend, the reader is referred to the Web version of this article.)

peak at 845.3 and 1020.0 nm, which are in the near-infrared region (NIR) of the electromagnetic spectrum, respectively (see Fig. 4). The absorption spectra of N-doped and 3N-doped GDY are slightly red shifted as compared to pristine GDY, respectively, but that of 2N-doped is blue shifted. The red shift in the absorption is observed at lower energy gap <1.55 eV, whereas the blue shift is observed at higher energy gap >1.55 eV. Consequently, the absorption shifts to lower wavelengths (higher energies) and higher wavelengths (lower energies) corresponds to blue and red shifts, respectively.

The $E_g^{opt}$ for the GDY and N-doped GDY nanomaterials is plotted in Fig. 5. $E_g^{opt.}$ can be calculated from UV–vis absorbance data using Tauc plot method [61], is defined as follows:

$$\alpha h\nu = K\left(h\nu - E_g^{opt.}\right)^n \tag{3}$$

where $\alpha$, $h\nu$ and $K$ are absorption coefficient, incident photon energy and energy independent constant, respectively, and $n$ is 2 for direct bandgap material and 1/2 for indirect bandgap nanomaterials. According to the analysis of the Tauc plot, GDY is a direct bandgap semiconductor with the $E_g^{opt}$ = 1.55 eV, in good agreement with previous studies [7,11,49,62,63]. $E_g^{opt}$ value decreases for N-GDY, but increases for 2N-GDY, and then sharply decreases for 3N-GDY (up to 0.78 eV). According to these results, the electronic character of N-doped GDY shows a semiconductor behavior with the $E_g^{opt}$ between 0.78 eV and 1.68 eV after N doping to GDY (see Fig. 5).

To gain information about chemical bonds and bond interactions, we performed the topological analysis of electron localization function (ELF) (see Fig. 6). The ELF analyses have a range of values between 0 and 1, where 0 and 1 values correspond to the absence of electrons and perfect localization, respectively [64]. Besides, ELF = 0.5 also corresponds to the free electron gas. Briefly, electrons are less localized as ELF values decrease. Thus, the nature of a bond could be transformed into a non-covalent type. ELF values of C–C bonds in GDY are in the range of 0.9 and 1.0, as seen in Fig. 6. This indicates that C–C bonds confirm the covalent bonding in GDY. Besides, as it is clear from the ELF contours calculated for the N-GDY, 2N-GDY and 3N-GDY, the electron localization also occurs in the center of the C–N and C–C

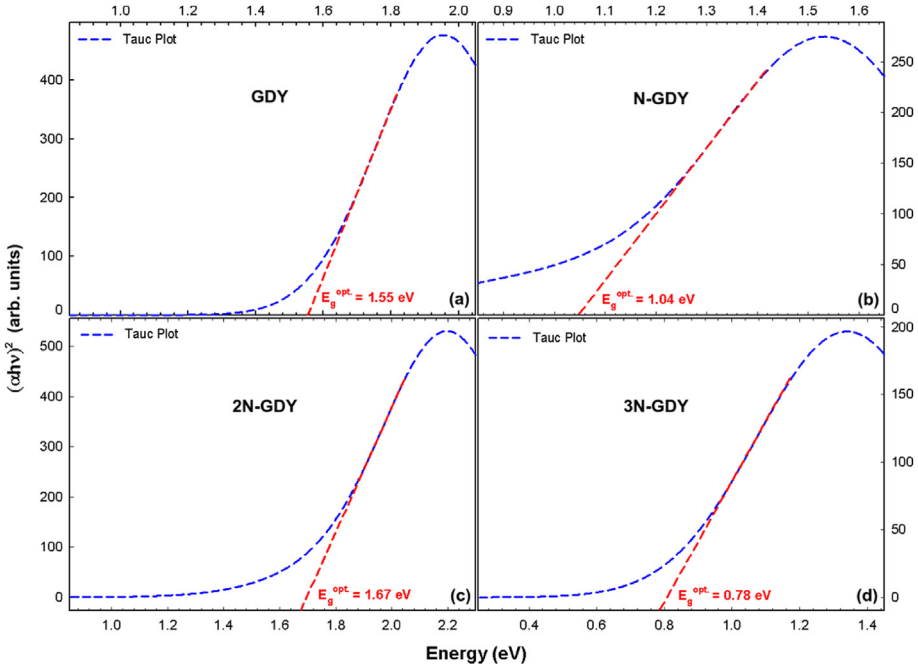


**Fig. 5.** (Colour online) Optical band gap of the GDY and N-doped GDY nanomaterials. (For interpretation of the references to color in this figure legend, the reader is referred to the Web version of this article.)

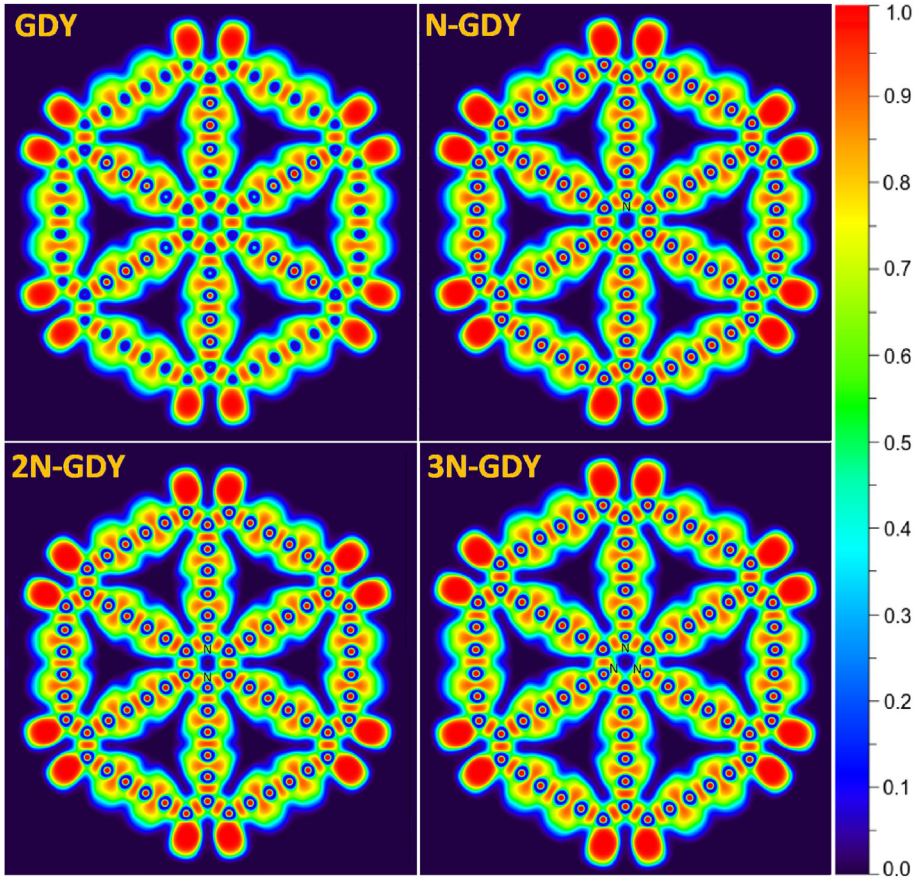


**Fig. 6.** (Colour online) Electron localization function (ELF) plots of the GDY and N-doped GDY nanomaterials. (For interpretation of the references to color in this figure legend, the reader is referred to the Web version of this article.)

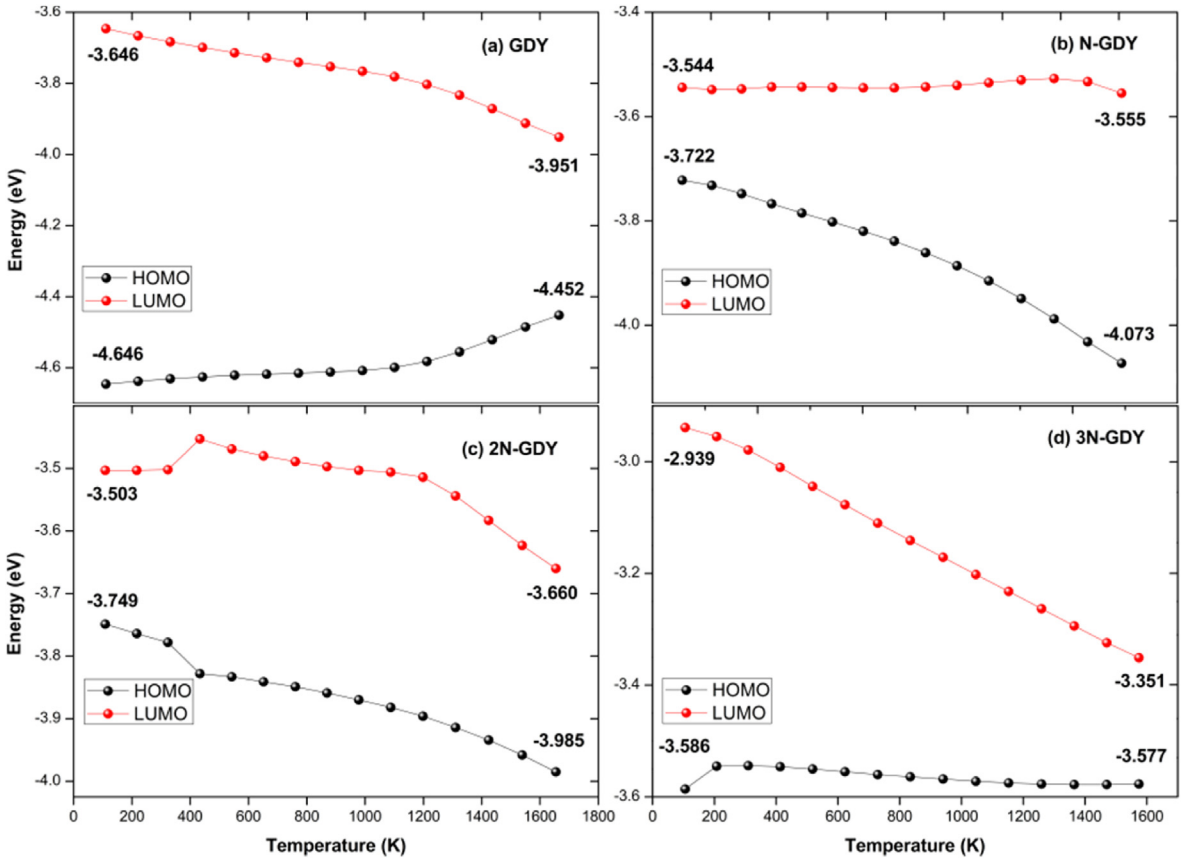


**Fig. 7.** The variations of the HOMO and LUMO energies of GDY and N-doped GDY nanomaterials as a function of temperature.

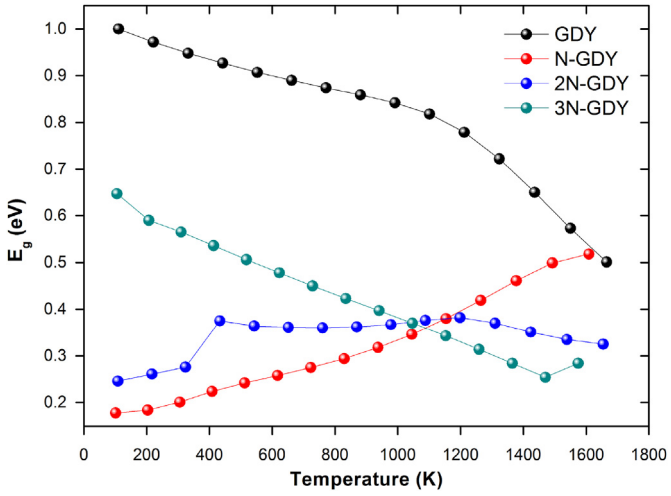


**Fig. 8.** (Colour online) The bandgaps of the GDY and N-doped GDY nanomaterials based on temperature. (For interpretation of the references to color in this figure legend, the reader is referred to the Web version of this article.)

bonds. For both pristine GDY and N-doped GDY, ELF values around the center of all C—C and C—N bonds are greater than 0.8. It confirms the covalent bonding in studied nanomaterials. These results are in excellent agreement with the literature [65]. We note that as the number of doped N atoms increases ELF analyses indicate an insignificant decrease in covalency of the C—C bond.

### 3.4. Temperature-dependent physical properties

Representative results from MD simulations are shown in Fig. S4 in Supporting information, where we plot the potential energy ($E_p$) curve versus temperature of the GDY and N-doped GDY nanomaterials. In each case the$E_p$ curve displays straight-line behavior in the range 100 K—1700 K. The $E_p$reflects the fact that the GDY without doping N has the larger the $E_p$ than N-doped GDY due to difference of the energy of atomic orbitals of C and N (see Fig. 2).

The changes in the HOMO and LUMO energy levels with temperature are shown in Fig. 7 (a, b, c and d) for the GDY and N-doped GDY nanomaterials. For GDY, the energy of the LUMO reduces from −3.646 eV to −3.951 eV, but the energy of the HOMO increases from −4.646 eV to −4.452 eV at 100 K and 1665 K, respectively (see Fig. 7(a) and Table S2 in Supporting information). As a result of these changes, the value of the $E_g$ slightly decreases up to about 1000 K and then it sharply decreases up to 1665 K due to increasing the intermolecular distance between C—C binary interactions and the lack of the symmetry in the chains (see Fig. S5 in Supporting information) of the GDY with temperature, as seen in Fig. 7. The decrease in the value of the $E_g$will give rise to an increase in the inhibition efficiency because the energy required to remove an electron from the last occupied orbital will be low [66]. On the other hand, after N doping, the value of LUMO decreases from −3.544 eV to −3.555 eV in the range of 101 K—1609 K for N-GDY, from −3.503 eV to −3.660 eV in the range of 108 K—1654 K for 2N-GDY and from −2.939 eV to −3.351 eV in the range of 105 K—1574 K for 3N-GDY. However, interesting chemistry is predicted that HOMO energy shows an increasing trend with temperature (see Fig. 7b, c and 7d). Therefore, we can conclude that the

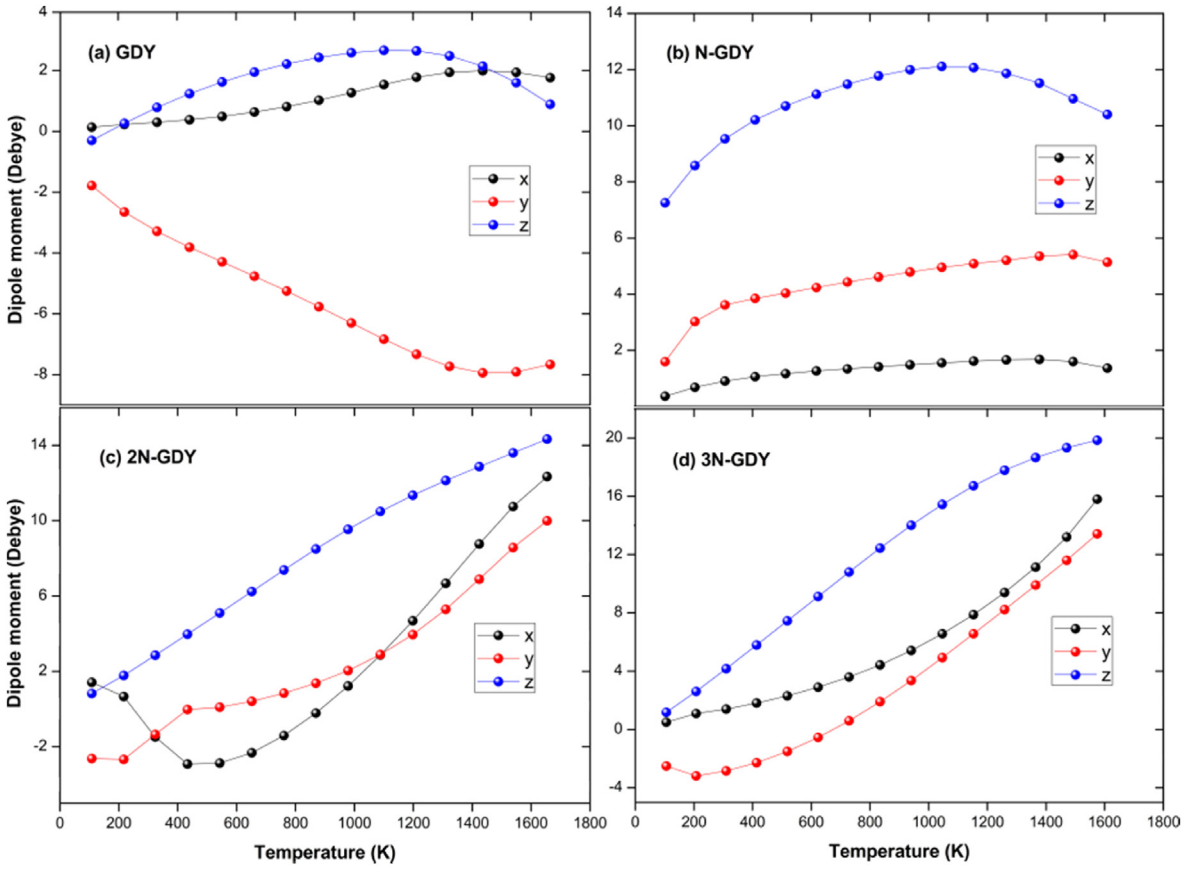


**Fig. 9.** The variations of the dipole moments of GDY and N-doped GDY nanomaterials in the x-, y- and z-directions as a function of temperature.

temperature causes a considerable shift in the relative position of the VB and CB. On the other hand, it is important to emphasize that an increase in the value of the $E_g$ is found linearly for N-GDY (see Fig. 8). For 2N-GDY, it is clearly shown the $E_g$ increase linearly up to 323 K and continues to increase with a sharp slope. After that, it remains almost constant up to almost 1000 K and then a decrease is observed at 1665 K. The nonmonotonic behavior of 2N-GDY at between 300 and 400 K, which destroys the linear dependence of the energy, is probably associated with the change in the bond distance and angle of *CCCCCC* chains. When it comes to 3N-GDY, the $E_g$ decreases approximately linearly. Here, the reason for the decrease in the $E_g$ for GDY and 3N-GDY can be explained with temperature-dependent electron-phonon interactions effectively determine semiconductor $E_g$ [67] due to variations of the bond energy which reflects the $E_g$. If the temperature is increased, the chemical bonding as electrons are promoted from VB to CB. On the other hand, the increase in the $E_g$ from 0.246 eV to 0.325 eV can be attributed to the Burstein moss effect. When the temperature is increased, all states near the CB are being populated. The Fermi energy level is pushed higher from −3.722 eV at 101 K to −4.027 eV at 1609 K, hence increasing the $E_g$.

Fig. 9 shows the variations of the dipole moment ($D_M$) of the GDY and N-doped GDY nanomaterials in the x-, y- and z-directions as a function of temperature. It is clearly shown that the-$D_M$ increases when increasing the content of N and temperature with the order GDY ˂ N-GDY < 2N-GDY < 3N-GDY. The GDY $D_M$ increases with temperature in negative z-directions and positive x- and z-directions up to almost 1400 K and then an increase was observed in three directions. With doping N, the $D_M$ increases in positive x-, y- and z-directions as a general trend. The increase in the $D_M$ may be related to the ability of the $D_M$ to bind an extra electron for high temperatures [66].

## 4. Conclusions

DFT/TD-DFT, LC—SCC—DFTB and MD simulations are employed to investigate the structural, electronic, reactivity and optical properties of pristine GDY and novel N-doped GDY nanomaterials. Pristine GDY, which is selected such as the basic building block of graphdiyne, has a stable quasi-planar geometry and consists of 6C-hexagon and 18C-hexagon. The N-GDY, 2N-GDY, and 3N-GDY are found to be structurally and chemically stable as GDY. Moreover, the $E_g$ of N-GDY, 2N-GDY, and 3N-GDY are found to be 0.15 eV, 0.22 eV and 0.98 eV, respectively, which are found compatible with LC—SCC—DFTB. These results indicate that the electronic character of GDY considerably changes from semiconductor to conductor with N-doping. However, the $E_g^{opt}$ calculations point out that N-doped GDY exhibits semiconducting electronic character, on the basis of TD-DFT calculations. More interestingly, the maximum UV—vis absorption spectra of the GDY and N-doped GDY nanomaterials indicate absorption peaks located in the range of 576.3 and 1020 nm in visible light or near-visible regions. It is noted that the absorption spectrum calculated by TD-DFT/CAM-B3LYP method for GDY agrees with the experimental results. According to ELF analyses of the GDY and N-doped GDY nanomaterials, the covalency of C—C and C—N bonds decreases depend on increasing the number of doped N atoms, but not large enough to affect their covalent bond. It is interesting to note that the decrease in the value of the $E_g$ with temperature for the GDY and 3 N GDY is observed, while an increase in the value of the $E_g$ with

temperature is found linearly for the N-GDY. The dipole moment increases when increasing the content of N and temperature. From obtained results, the N-doped GDY nanomaterials with porous and planar structures could open up an opportunity to develop storage materials with high capacity.

## CRediT authorship contribution statement

**İskender Muz:** Investigation, Methodology, Visualization, Writing - original draft, Writing - review & editing, Data curation, Software. **Mustafa Kurban:** Supervision, Investigation, Methodology, Conceptualization, Writing - original draft, Writing - review & editing, Data curation, Validation, Software.

## Declaration of competing interest

The authors declare that they have no known competing financial interests or personal relationships that could have appeared to influence the work reported in this paper.

## Acknowledgments

The numerical calculations reported were partially performed at TUBITAK ULAKBIM, High Performance and Grid Computing Center (TRUBA resources), Turkey.

## Appendix A. Supplementary data

Supplementary data to this article can be found online at https://doi.org/10.1016/j.jallcom.2020.155983.

## References

[1] M.M. Haley, S.C. Brand, J.J. Pak, Carbon networks based on dehydrobenzoannulenes: synthesis of graphdiyne substructures, Angew. Chem. Int. Ed. 36 (1997) 836–838, https://doi.org/10.1002/anie.199708361.
[2] X. Gao, H. Liu, D. Wang, J. Zhang, Graphdiyne: synthesis, properties, and applications, Chem. Soc. Rev. 48 (2019) 908–936, https://doi.org/10.1039/c8cs00773j.
[3] S. Zhang, H. Du, J. He, C. Huang, H. Liu, G. Cui, Y. Li, Nitrogen-doped graphdiyne applied for lithium-ion storage, ACS Appl. Mater. Interfaces 8 (2016) 8467–8473, https://doi.org/10.1021/acsami.6b00255.
[4] S. Wang, L. Yi, J.E. Halpert, X. Lai, Y. Liu, H. Cao, R. Yu, D. Wang, Y. Li, A novel and highly efficient photocatalyst based on P25-graphdiyne nanocomposite, Small 8 (2012) 265–271, https://doi.org/10.1002/smll.201101686.
[5] C. Sun, D.J. Searles, Lithium storage on graphdiyne predicted by DFT calculations, J. Phys. Chem. C 116 (2012) 26222–26226, https://doi.org/10.1021/jp309638z.
[6] A. Farokh Niaei, T. Hussain, M. Hankel, D. Searles, Sodium-intercalated bulk graphdiyne as an anode material for rechargeable batteries, J. Power Sources 343 (2017) 354–363, https://doi.org/10.1016/jjpowsour.2017.01.027.
[7] Y. Jiao, A. Du, M. Hankel, Z. Zhu, V. Rudolph, S.C. Smith, Graphdiyne: a versatile nanomaterial for electronics and hydrogen purification, Chem. Commun. 47 (2011) 11843–11845, https://doi.org/10.1039/C1CC15129K.
[8] M. Zhang, X. Wang, H. Sun, N. Wang, Q. Lv, W. Cui, Y. Long, C. Huang, Enhanced paramagnetism of mesoscopic graphdiyne by doping with nitrogen, Sci. Rep. 7 (2017) 11535, https://doi.org/10.1038/s41598-017-11698-9.
[9] J. He, S.Y. Ma, P. Zhou, C.X. Zhang, C. He, L.Z. Sun, Magnetic properties of single transition-metal atom absorbed graphdiyne and graphyne sheet from DFT plus U calculations, J. Phys. Chem. C 116 (2012) 26313–26321, https://doi.org/10.1021/jp307408u.
[10] G. Li, Y. Li, H. Liu, Y. Guo, Y. Li, D. Zhu, Architecture of graphdiyne nanoscale films, Chem. Commun. 46 (2010) 3256–3258, https://doi.org/10.1039/B922733D.
[11] M. Long, L. Tang, D. Wang, Y. Li, Z. Shuai, Electronic structure and carrier mobility in graphdiyne sheet and nanoribbons: theoretical predictions, ACS Nano 5 (2011) 2593–2600, https://doi.org/10.1021/nn102472s.
[12] L. Sun, P.H. Jiang, H.J. Liu, D.D. Fan, J.H. Liang, J. Wei, L. Cheng, J. Zhang, J. Shi, Graphdiyne, A two-dimensional thermoelectric material with high figure of merit, Carbon N. Y. 90 (2015) 255–259, https://doi.org/10.1016/j.carbon.2015.04.037.
[13] C. Lu, Y. Yang, J. Wang, R. Fu, X. Zhao, L. Zhao, Y. Ming, Y. Hu, H. Lin, X. Tao, Y. Li, W. Chen, High-performance graphdiyne-based electrochemical actuators, Nat. Commun. 9 (2018) 752, https://doi.org/10.1038/s41467-018-03095-1.
[14] K. Krishnamoorthy, S. Thangavel, J.C. Veetil, N. Raju, G. Venugopal, S.J. Kim, Graphdiyne nanostructures as a new electrode material for electrochemical supercapacitors, Int. J. Hydrogen Energy 41 (2016) 1672–1678, https://doi.org/10.1016/j.ijhydene.2015.10.118.
[15] H. Shang, Z. Zuo, Y. Li, Highly lithiophilic graphdiyne nanofilm on 3D free-standing Cu nanowires for high-energy-density electrodes, ACS Appl. Mater. Interfaces 11 (2019) 17678–17685, https://doi.org/10.1021/acsami.9b03633.
[16] L. Li, Z. Zuo, H. Shang, F. Wang, Y. Li, In-situ constructing 3D graphdiyne as all-carbon binder for high-performance silicon anode, Nanomater. Energy 53 (2018) 135–143, https://doi.org/10.1016/j.nanoen.2018.08.039.
[17] S. Thangavel, K. Krishnamoorthy, V. Krishnaswamy, N. Raju, S.J. Kim, G. Venugopal, Graphdiyne-ZnO nanohybrids as an advanced photocatalytic material, J. Phys. Chem. C 119 (2015) 22057–22065, https://doi.org/10.1021/acs.jpcc.5b06138.
[18] M. Kurban, İ. Muz, Theoretical investigation of the adsorption behaviors of fluorouracil as an anticancer drug on pristine and B-, Al-, Ga-doped C36 nanotube, J. Mol. Liq. 309 (2020) 113209, https://doi.org/10.1016/j.molliq.2020.113209.
[19] S.-S. Yu, W.-T. Zheng, Effect of N/B doping on the electronic and field emission properties for carbon nanotubes, carbon nanocones, and graphene nanoribbons, Nanoscale 2 (2010) 1069–1082, https://doi.org/10.1039/c0nr00002g.
[20] B.K. Jiang, A.Y. Chen, J.F. Gu, J.T. Fan, Y. Liu, P. Wang, H.J. Li, H. Sun, J.H. Yang, X.Y. Wang, Corrosion resistance enhancement of magnesium alloy by N-doped graphene quantum dots and polymethyltrimethoxysilane composite coating, Carbon N. Y. 157 (2020) 537–548, https://doi.org/10.1016/j.carbon.2019.09.013.
[21] Y. Li, W. Ma, J. Sun, M. Lin, Y. Niu, X. Yang, Y. Xu, Electrochemical generation of Fe3C/N-doped graphitic carbon nanozyme for efficient wound healing in vivo, Carbon N. Y. 159 (2020) 149–160, https://doi.org/10.1016/j.carbon.2019.11.093.
[22] X. Qin, Y. Huang, K. Wang, T. Xu, S. Li, M. Zhao, Y. Wang, Q. Chen, Novel hexagonal Bi2O2CO3 porous nanoplate/nitrogen-doped graphene nanomaterials with enhanced electrochemical properties for oxygen reduction reaction in acidic media for fuel cells, Carbon N. Y. 152 (2019) 459–473, https://doi.org/10.1016/j.carbon.2019.06.028.
[23] N. Wanninayake, Q. Ai, R. Zhou, M.A. Hoque, S. Herrell, M. Guzman I, C. Risko, D.Y. Kim, Understanding the effect of host structure of nitrogen doped ultrananocrystalline diamond electrode on electrochemical carbon dioxide reduction, Carbon N. Y. 157 (2020) 408–419, https://doi.org/10.1016/j.carbon.2019.10.022.
[24] M. Kurban, Electronic structure, optical and structural properties of Si, Ni, B and N-doped a carbon nanotube: DFT study, Optik 172 (2018) 295–301, https://doi.org/10.1016/j.ijleo.2018.07.028.
[25] H. Shang, Z. Zuo, H. Zheng, K. Li, Z. Tu, Y. Yi, H. Liu, Y. Li, Y. Li, N-doped graphdiyne for high-performance electrochemical electrodes, Nanomater. Energy 44 (2018) 144–154, https://doi.org/10.1016/j.nanoen.2017.11.072.
[26] X. Shen, Z. Yang, K. Wang, N. Wang, J. He, H. Du, C. Huang, Nitrogen-doped graphdiyne as high-capacity electrode materials for both lithium-ion and sodium-ion capacitors, ChemElectroChem 5 (2018) 1435–1443, https://doi.org/10.1002/celc.201800300.
[27] Q. Lv, W. Si, J. He, L. Sun, C. Zhang, N. Wang, Z. Yang, X. Li, X. Wang, W. Deng, Y. Long, C. Huang, Y. Li, Selectively nitrogen-doped carbon materials as superior metal-free catalysts for oxygen reduction, Nat. Commun. 9 (2018) 3376, https://doi.org/10.1038/s41467-018-05878-y.
[28] Q. Lv, W. Si, Z. Yang, N. Wang, Z. Tu, Y. Yi, C. Huang, L. Jiang, M. Zhang, J. He, Y. Long, Nitrogen-doped porous graphdiyne: a highly efficient metal-free electrocatalyst for oxygen reduction reaction, ACS Appl. Mater. Interfaces 9 (2017) 29744–29752, https://doi.org/10.1021/acsami.7b08115.
[29] Y. Ma, J. Lin, X.-N. Song, C.-K. Wang, W. Hua, Y. Luo, Local structures of nitrogen-doped graphdiynes determined by computational X-ray spectroscopy, Carbon N. Y. 149 (2019) 672–678, https://doi.org/10.1016/j.carbon.2019.04.045.
[30] M.J. Frisch, G.W. Trucks, H.B. Schlegel, G.E. Scuseria, M.A. Robb, J.R. Cheeseman, G. Scalmani, V. Barone, B. Mennucci, G.A. Petersson, H. Nakatsuji, M. Caricato, X. Li, H.P. Hratchian, A.F. Izmaylov, J. Bloino, G. Zheng, J.L. Sonnenberg, M. Hada, M. Ehara, K. Toyota, R. Fukuda, J. Hasegawa, M. Ishida, T. Nakajima, Y. Honda, O. Kitao, H. Nakai, T. Vreven, J.A. Montgomery, J.E. Peralta, F. Ogliaro, M. Bearpark, J.J. Heyd, E. Brothers, K.N. Kudin, V.N. Staroverov, R. Kobayashi, J. Normand, K. Raghavachari, A. Rendell, J.C. Burant, S.S. Iyengar, J. Tomasi, M. Cossi, N. Rega, J.M. Millam, M. Klene, J.E. Knox, J.B. Cross, V. Bakken, C. Adamo, J. Jaramillo, R. Gomperts, R.E. Stratmann, O. Yazyev, A.J. Austin, R. Cammi, C. Pomelli, J.W. Ochterski, R.L. Martin, K. Morokuma, V.G. Zakrzewski, G.A. Voth, P. Salvador, J.J. Dannenberg, S. Dapprich, A.D. Daniels, Farkas, J.B. Foresman, J. V Ortiz, J. Cioslowski, D.J. Fox, Gaussian 09, Revision E.01, Gaussian Inc., Wallingford CT, 2009.
[31] A.D. Becke, Density-functional thermochemistry. III. the role of exact exchange, J. Chem. Phys. 98 (1993) 5648–5652, https://doi.org/10.1063/1.464913.
[32] A.D. Becke, Density-functional exchange-energy approximation with correct asymptotic-behavior, Phys. Rev. 38 (1988) 3098–3100, https://doi.org/10.1103/PhysRevA.38.3098.
[33] V.N. Staroverov, G.E. Scuseria, J. Tao, J.P. Perdew, Comparative assessment of a new nonempirical density functional: molecules and hydrogen-bonded complexes, J. Chem. Phys. 119 (2003) 12129–12137, https://doi.org/10.1063/1.1626543.

[34] R.G. Pearson, The principle of maximum hardness, Acc. Chem. Res. 26 (1993) 250–255, https://doi.org/10.1021/ar00029a004.
[35] R.G. Parr, R.G. Pearson, Absolute hardness - companion parameter to absolute electronegativity, J. Am. Chem. Soc. 105 (1983) 7512–7516, https://doi.org/10.1021/ja00364a005.
[36] N.M. O'Boyle, A.L. Tenderholt, K.M. Langner, cclib, A library for package-independent computational chemistry algorithms, J. Comput. Chem. 29 (2008) 839–845, https://doi.org/10.1002/jcc.20823.
[37] T. Yanai, D.P. Tew, N.C. Handy, A new hybrid exchange–correlation functional using the Coulomb-attenuating method (CAM-B3LYP), Chem. Phys. Lett. 393 (2004) 51–57, https://doi.org/10.1016/j.cplett.2004.06.011.
[38] B. Aradi, B. Hourahine, T. Frauenheim, DFTB+, a sparse matrix-based implementation of the DFTB method, J. Phys. Chem. 111 (2007) 5678–5684, https://doi.org/10.1021/jp070186p.
[39] V.Q. Vuong, J.A. Kuriappan, M. Kubillus, J.J. Kranz, T. Mast, T.A. Niehaus, S. Irle, M. Elstner, Parametrization and benchmark of long-range corrected DFTB2 for organic molecules, J. Chem. Theor. Comput. 14 (2018) 115–125, https://doi.org/10.1021/acs.jctc.7b00947.
[40] H.C. Andersen, Molecular-dynamics simulations at constant pressure and-or temperature, J. Chem. Phys. 72 (1980) 2384–2393, https://doi.org/10.1063/1.439486.
[41] L. Verlet, Computer "Experiments" on classical fluids. I. thermodynamical properties of Lennard-Jones molecules, Phys. Rev. 159 (1967) 98–103, https://doi.org/10.1103/PhysRev.159.98.
[42] A. Seif, M.J. López, A. Granja-DelRío, K. Azizi, J.A. Alonso, Adsorption and growth of palladium clusters on graphdiyne, Phys. Chem. Chem. Phys. 19 (2017) 19094–19102, https://doi.org/10.1039/C7CP03263C.
[43] N. Narita, S. Nagai, S. Suzuki, K. Nakao, Optimized geometries and electronic structures of graphyne and its family, Phys. Rev. B 58 (1998) 11009–11014, https://doi.org/10.1103/PhysRevB.58.11009.
[44] Y. Pei, Mechanical properties of graphdiyne sheet, Phys. B Condens. Matter 407 (2012) 4436–4439, https://doi.org/10.1016/j.physb.2012.07.026.
[45] S. Jalili, F. Houshmand, J. Schofield, Study of carrier mobility of tubular and planar graphdiyne, Appl. Phys. A 119 (2015) 571–579, https://doi.org/10.1007/s00339-015-8992-8.
[46] M. Ebadi, A. Reisi-Vanani, F. Houshmand, P. Amani, Calcium-decorated graphdiyne as a high hydrogen storage medium: evaluation of the structural and electronic properties, Int. J. Hydrogen Energy 43 (2018) 23346–23356, https://doi.org/10.1016/j.ijhydene.2018.10.205.
[47] Z. Lu, S. Li, P. Lv, C. He, D. Ma, Z. Yang, First principles study on the interfacial properties of NM/graphdiyne (NM = Pd, Pt, Rh and Ir): the implications for NM growing, Appl. Surf. Sci. 360 (2016) 1–7, https://doi.org/10.1016/j.apsusc.2015.10.219.
[48] V. Nagarajan, R. Chandiramouli, Investigation of NH 3 adsorption behavior on graphdiyne nanosheet and nanotubes: a first-principles study, J. Mol. Liq. 249 (2018) 24–32, https://doi.org/10.1016/j.molliq.2017.11.007.
[49] H. Bu, M. Zhao, A. Wang, X. Wang, First-principles prediction of the transition from graphdiyne to a superlattice of carbon nanotubes and graphene nanoribbons, Carbon N. Y. 65 (2013) 341–348, https://doi.org/10.1016/j.carbon.2013.08.035.
[50] G.L. Harris, Properties of Silicon Carbide, IEE, INSPEC., London, U.K, 1995. London, http://books.google.com/books?id=279TAAAAMAAJ.
[51] G. Luo, X. Qian, H. Liu, R. Qin, J. Zhou, L. Li, Z. Gao, E. Wang, W.-N. Mei, J. Lu, Y. Li, S. Nagase, Quasiparticle energies and excitonic effects of the two-dimensional carbon allotrope graphdiyne: theory and experiment, Phys. Rev. B 84 (2011), 075439, https://doi.org/10.1103/PhysRevB.84.075439.
[52] M.S. Hybertsen, S.G. Louie, Electron correlation in semiconductors and insulators - band-gaps and quasi-particle energies, Phys. Rev. B 34 (1986) 5390–5413, https://doi.org/10.1103/PhysRevB.34.5390.
[53] B. Streetman, S. Banerjee, Solid State Electronic Devices, fifth ed., Prentice Hall, Upper Saddle River, N.J., 2000.
[54] S. Zhang, J. He, J. Zheng, C. Huang, Q. Lv, K. Wang, N. Wang, Z. Lan, Porous graphdiyne applied for sodium ion storage, J. Mater. Chem. A. 5 (2017) 2045–2051, https://doi.org/10.1039/c6ta09822c.
[55] F. Diederich, Carbon scaffolding - building acetylenic all-carbon and carbon-rich compounds, Nature 369 (1994) 199–207, https://doi.org/10.1038/369199a0.
[56] C. Zhao, X. Zhou, S. Xie, H. Wei, J. Chen, X. Chen, C. Chen, DFT study of electronic structure and properties of N, Si and Pd-doped carbon nanotubes, Ceram. Int. 44 (2018) 21027–21033, https://doi.org/10.1016/j.ceramint.2018.08.138.
[57] S.S. Yu, Q.B. Wen, W.T. Zheng, Q. Jiang, Effects of doping nitrogen atoms on the structure and electronic properties of zigzag single-walled carbon nanotubes through first-principles calculations, Nanotechnology 18 (2007) 165702, https://doi.org/10.1088/0957-4484/18/16/165702.
[58] I. Muz, M. Kurban, A comprehensive study on electronic structure and optical properties of carbon nanotubes with doped B, Al, Ga, Si, Ge, N, P and as and different diameters, J. Alloys Compd. 802 (2019) 25–35, https://doi.org/10.1016/j.jallcom.2019.06.210.
[59] N. Yang, Y. Liu, H. Wen, Z. Tang, H. Zhao, Y. Li, D. Wang, Photocatalytic properties of graphdiyne and graphene modified TiO2: from theory to experiment, ACS Nano 7 (2013) 1504–1512, https://doi.org/10.1021/nn305288z.
[60] L. Wu, Y. Dong, J. Zhao, D. Ma, W. Huang, Y. Zhang, Y. Wang, X. Jiang, Y. Xiang, J. Li, Y. Feng, J. Xu, H. Zhang, Kerr nonlinearity in 2D graphdiyne for passive photonic diodes, Adv. Mater. 31 (2019) 1807981, https://doi.org/10.1002/adma.201807981.
[61] J. Tauc, R. Grigorovici, A. Vancu, Optical properties and electronic structure of amorphous germanium, Phys. Status Solidi B 15 (1966) 627–637, https://doi.org/10.1002/pssb.19660150224.
[62] K. Srinivasu, S.K. Ghosh, Graphyne and graphdiyne: promising materials for nanoelectronics and energy storage applications, J. Phys. Chem. C 116 (2012) 5951–5956, https://doi.org/10.1021/jp212181h.
[63] A.N. Enyashin, A.L. Ivanovskii, Graphene allotropes, Phys. Status Solidi B 248 (2011) 1879–1883, https://doi.org/10.1002/pssb.201046583.
[64] B. Silvi, A. Savin, Classification of chemical-bonds based on topological analysis of electron localization functions, Nature 371 (1994) 683–686, https://doi.org/10.1038/371683a0.
[65] B. Mortazavi, M. Makaremi, M. Shahrokhi, Z. Fan, T. Rabczuk, N-graphdiyne two-dimensional nanomaterials: semiconductors with low thermal conductivity and high stretchability, Carbon N. Y. 137 (2018) 57–67, https://doi.org/10.1016/j.carbon.2018.04.090.
[66] G. Gece, Theoretical evaluation of the inhibition properties of two thiophene derivatives on corrosion of carbon steel in acidic media, Mater. Corros. Und Korrosion. 64 (2013) 940–944, https://doi.org/10.1002/maco.201106482.
[67] H.Y. Fan, Temperature dependence of the energy gap in semiconductors, Phys. Rev. 82 (1951) 900–905, https://doi.org/10.1103/PhysRev.82.900.